VNU Journal of Science: Earth and Environmental Sciences

Journal homepage: https://js.vnu.edu.vn/EES

Original Article

Numerical Simulation of the Impact Response of Super Typhoon Rammasun (2014) on Hydrodynamics and Suspended Sediment in the Gulf of Tonkin

Le Duc Cuong[1,2,*], Do Huy Toan[3], Dao Dinh Cham[1], Nguyen Ba Thuy[4], Du Van Toan[5], Nguyen Minh Huan[3], Nguyen Quoc Trinh[1], Tran Anh Tu[6], Le Xuan Sinh[6]

[1]*Institute of Geography, VAST, Building A27, 18 Hoang Quoc Viet, Cau Giay, Hanoi, Vietnam*
[2]*Graduate University of Science and Technology, Building A28, 18 Hoang Quoc Viet, Cau Giay, Hanoi*
[3]*VNU University of Science, 334 Nguyen Trai, Thanh Xuan, Hanoi, Vietnam*
[4]*Vietnam National Hydro-meteorological Forecasting Center, 8 Phao Dai Lang, Dong Da, Hanoi, Vietnam*
[5]*Vietnam institute of Seas and Islands, VASI, 67 Chien Thang, Thanh Xuan, Hanoi, Vietnam*
[6]*Institute of Marine Environment and Resources, VAST, 246 Da Nang, Ngo Quyen, Hai Phong, Vietnam*

Received 15 September 2020
Revised 26 January 2021; Accepted 02 February 2021

Abstract: In the present study, an open-source coupled numerical model based on Delft3D source code was performed and applied to simulate the hydrodynamic changes due to the Super Typhoon Rammasun in the Gulf of Tonkin (GTK). The results indicated that the typhoon strongly affects the current, water level, wave fields, and suspended sediment transport in the western coastal areas of the GTK. The simulated wave height field reflects the wavefield caused by the Super Typhoon Rammasun, and the maximum wave height was 6.8m during the Typhoon Rammasun event. The current is affected by the strong wind caused due to the typhoon in the surface layer. Accordingly, current velocity and significant wave height increased distinctly by 4 and 9 times, respectively, more than the normal condition. In the western coastal areas, the maximum sea level falls to about 0.7m, and the current velocity was 0.25-0.3m/s (during ebb tide stages) greater than it was in normal conditions during Super Typhoon Rammasun event. The moving Super Typhoon Rammasun resulted in suspended sediment concentration (SSC) increasing by 2 times more than normal monsoon conditions and also strengthened suspended sediment transport in the GTK, which was mostly controlled by strong waves during typhoon events. Simulated results showed that SSC in the GTK varied dramatically in temporal and spatial distribution, with the maximum value in wet seasons because of large sediment discharge around the river mouth.

Keywords: Gulf of Tonkin, Delf3D, Typhoon Rammasun, Hydrodynamics, Suspended Sediment.

* Corresponding author.
E-mail address: lyecuong238@gmail.com

https://doi.org/10.25073/2588-1094/vnuees.4687

1. Introduction

The number of typhoons and tropical cyclones that approached or affected Vietnam during the 20th century is roughly counted at 786, of which 348 are typhoons with wind speeds greater than 120 km/h [1]. The western coastal areas of GTK are a complex tidal estuary with many channels and shoals, which were affected by typhoons frequently. In this study, we conducted a statistical analysis of Typhoons passing through the GTK from July to September (2014), and we also examined a representative case, Super Typhoon Rammasun, which impacted strongly on the hydrodynamic and sediment transport around the Red River mouth. The history of typhoons (1951-2016) and the risk of the typhoon and storm surge in coastal areas of Vietnam are analyzed and evaluated based on the observation data, results of statistical and numerical models [2]. Numerical modeling of sediment transport has been recognized as a valuable tool for understanding the suspended sediment process [3]. There have been some previous studies are related to tropical cyclones in Vietnam [4] and [5].

Super Typhoon Rammasun was one of the only two super typhoons on record in the East Vienam Sea, with the other one being Pamela in 1954. With the maximum sustained wind velocity of 46.3 m/s and a central pressure of 935 hPa, Typhoon Rammasun passed through the northeastern Hainan Island on 18 July 2014. It had destructive impacts on the Philippines, South China, and Vietnam.

According to the site survey data and based on the JMA's historical tropical cyclone tracks data, an open-source coupled numerical model was established and validated, which simulates the hydrodynamic conditions due to Super Rammasun Typhoon in the GTK. We aim to simulate the coastal hydrodynamic characteristics (mainly tide, wind driven surge, and pressure surge) and wind induced wave effects. Furthermore, the applicability of the open-source modeling methods to simulate the typhoon together with Tide-Flow-Wave and sediment transport coupled modeling system was assessed as the main objective of this study. By using both approaches, we attempted to reproduce and simulate the impact of the typhoon on hydrodynamics and suspended sediment transport in GTK.

2. Data and Methods

2.1. Data

The database used in this study are as below:

- Coastlines used Global Self-consistent, Hierarchical, High-resolution Geography Database (GSHHG), version 2.3.7 published by the National Centers for Environmental Information (NOAA). GSHHG is a high-resolution geography data set, amalgamated from two databases: World Vector Shorelines (WVS) with 1:250000 scale and CIA World Data Bank II (WDBII). The GSHHG data is processed and assembled by Wessel et al., [6].

- Bathymetric was digitized from topography maps over the Western coastal zone of Gulf of Tonkin with 1:50000 scale (published by the Department of Survey and Mapping, Ministry of Environment and resources, Vietnam). Bathymetry in the offshore area used bathymetry database of Gebco-2014 (General Bathymetric Chart of the Ocean) with 30-arc second high resolution from the British Oceanographic Data Centre (BODC) [7]. The bathymetry model that has been used as an underlying base grid in Gebco-2014 is version 5.0 of SRTM30_PLUS [8]. This model has a grid cell spacing of 30 arcsec and extends between 90°N and 90°S. It has been compiled from more than 290 million edited soundings and version 11.1 of Smith and Sandwell's bathymetry grid [9] and [10].

- Tides and their dynamic processes were studied by assimilating Topex/Poseidon altimetry data into a barotropic ocean tides model for the eight major constituents. A tidal data inversion scheme “TPXO 8.0 Global” with 30-second resolutions was used [11].

- The in-situ evolution of the data was analyzed using station measurements at the open boundaries in the rivers provided by the Institute

of Marine Environment and Resources (Vietnam), which are included water river discharge, water temperature, salinity, current velocity and SSC.

- Wind data and background atmospheric pressure used in this study are extracted from the global climate model CFSR (Climate Forecast System Reanalysis) of the National Centers for Environmental Prediction – National Oceanic and Atmospheric Administration (NCEP/ NOAA) with a horizontal resolution down to one-half of a degree (approximately 56 km).

- Data on typhoons, tropical depressions (Storm trajectories and storm parameters) affecting the GTK were collected from Japanese meteorological agency. The tropical cyclones data over the GTK were from JMA best track dataset, which provides TCs location and intensity at 6-hour intervals, and then the wind and atmospheric pressure field data of the Typhoon Rammasun were exploited from TC tracks [12].

- The monthly salinity and temperature mean at sea open boundaries with the resolutions of these are 1° × 1° drawn from the website of Asia-Pacific Data-Research Center

- Wave data at open boundary were analyzed using the daily, WAVEWATCH-III high resolutions dataset drawn from the website of APDRC.

- Data for model verification: Based on the water level, it was recorded at tidal stations along the coast in the GTK for model verification. The SSC data derived from observations by IMER' projects (Vietnam) at in-situ stations in 2013 and 2014.

2.1. Methods

In this study, a nested and coupled model which combines a typhoon model, hydrodynamic model (Delft3D-FLOW), wave model (Delft3D-WAVE) and sediment transport model (Delft3D-SED) were applied.

- Flow model (Delft3D-FLOW): the FLOW module is the heart of Delft3D and is a multi-dimensional (2D or 3D) hydrodynamic (and transport) simulation program that calculate non-steady flow and transport phenomena resulting from the tidal and meteorological force on a curvilinear, boundary fitted grid or spherical coordinates. The numerical hydrodynamic modeling system Delft3D-FLOW can be used to solve unsteady shallow water equations in two (depth-averaged) or three dimensions. The system of equations consists of the horizontal equations of motion, the continuity equation, and the transport equations for conserved constituents [13]. The depth-averaged continuity equation is given by:

$$\frac{\partial \zeta}{\partial t}\frac{1}{\sqrt{G_{\xi\xi}}\sqrt{G_{\eta\eta}}}\frac{\partial\left[(d+\zeta)U\sqrt{G_{\eta\eta}}\right]}{\partial \xi}+\frac{1}{\sqrt{G_{\xi\xi}}\sqrt{G_{\eta\eta}}}\frac{\partial\left[(d+\zeta)V\sqrt{G_{\eta\eta}}\right]}{\partial \xi}=Q \qquad (1)$$

Where ξ and η represent the horizontal coordinates in the orthogonal curvilinear coordinate system; $\sqrt{G_{\xi\xi}}\ and\ \sqrt{G_{\eta\eta}}$represent the systems used to convert the parameters from the orthogonal curvilinear coordinate system to the Cartesian coordinate system; d represents the depth at the point of calculation (compared with 0 m on the charts); ζ represents the water level at the point of the calculation (compared with 0 m on the charts); U and V represent the average velocity components in the ξ and η directions, respectively; Q representing the contributions per unit area due to the discharge or withdrawal of water.

- Wave model (Delft3D-WAVE): the wave model SWAN is available in the wave module of Delft3D. This is a third-generation wave model [14]. The previously available HISWA wave model was a second-generation wave model [15]. Delft3D-WAVE is a model used to simulate the propagation and transformation of the wave energy from given initial environmental conditions of waves and wind over arbitrary bottom depths. In the research version, the waves are phase-averaged over the high-frequency swell, but the gravity band waves are phase resolved. HISWA solves for C_g and θ using the initial conditions and

bathymetry. The shortwave energy, E_W, is solved through the energy flux balances given by:

$$\frac{\partial E_w}{\partial t} + \frac{\partial E_w c_g \cos(\theta)}{\partial x} + \frac{\partial E_w c_g \cos(\theta)}{\partial y} = -D_w \quad (2)$$

here c_g is the group velocity, θ is the incidence angle with respect to the x-axis, x is the distance in the cross-shore, y is the distance in the alongshore, and D_w is the wave energy dissipation.

- Sediment Transport Model (Delft3D-SED)

The research model computes sediment transport on the same scale as the flow. An advection/diffusion equation model is used for sediment transport [16] and [17].

$$\frac{\partial}{\partial t} hC + \frac{\partial}{\partial x} hCu^E + \frac{\partial}{\partial y} hCv^E = \frac{hC_{eq} - hC}{T_s} \quad (3)$$

where C is the sediment concentration, w_s is sediment fall velocity, and Ts is the adaptation time for the diffusion of the sediment given by,

$$T_s = 0.05 \frac{h}{w_s}$$

The equilibrium sediment concentration is obtained by the Soulsby-van Rijn sediment transport formulation [15].

$$C_{eq} = \frac{\rho(A_{sb} + A_{ss})}{h} \left(((\bar{u}^E + \bar{v}^E)^2 + \frac{.018 u_{rms}^2}{C_d})^{\frac{1}{2}} - u_{cr} \right)^{2.4} (1 - 3.5m) \quad (4)$$

Where A_{sb} and A_{ss} are the bed load coefficients which are a function of the sediment grain size, relative density of the sediment, and the local water depth [18]. To include infra gravity velocities in the sediment stirring requires a recalibration of A_{sb} and A_{ss}. C_d is the drag coefficient; u_{cr} is the critical threshold that the mean and orbital velocities must surpass to stir sediment. $\bar{u}^E$ and $\bar{v}^E$ are the mean Eulerian velocities (averaged over many wave groups) that stir the sediment, and u_{rms} is the combined wave breaking induced turbulence motion and near-bed short wave velocity.

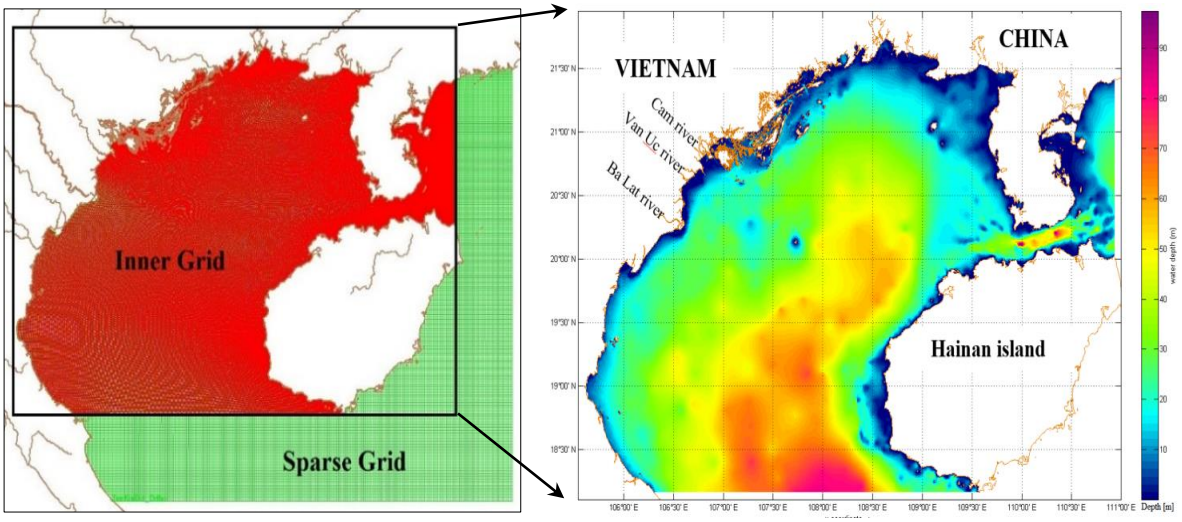

Figure 1. The model domain, grids and bathymetry.

- Model setup: the domain and grids having been selected for the modeling are shown in Figure 1. The sparse model grid consists of 341 × 218 grid cells with a resolution of approximately 2.0 km. The high-resolution model grid is nested inside the outer model domain, which is limited from 105.6 ^{0}E to 111.1 ^{0}E and from 18.0 ^{0}N to 22.0 ^{0}N. The inner orthogonal curvilinear grid used in the nested model area was designed to match the complicated coastline. The inner model grid consists of 488×705 grid cells, which have a high

resolution in the area of coastal. In the northern part and offshore area, the cells become more elongated where the coastal areas have a length of 250-350 m of grids. The offshore area has a resolution of approximately 500-600 m of grid cells.

Simulation of hydrodynamics and sediment transport caused by typhoon uses a meteorology-wave-storm surge-tide coupled model (online coupling with hydrodynamics and sediment transport). The simulations start with constant values, the initial conditions of the current velocities were set to be zero uniforms, the initial surface water elevation at the beginning of simulation is set to be zero uniforms. The harmonic constants of 13 tidal constituents (M2, S2, K2, N2, O1, K1, P1, Q1, MF, MM, M4, MS4, MN4) are considered to be the open sea boundary of input data. The appropriate river discharge boundaries are adjusted based on monthly-averaged discharge data recorded. Wave boundary conditions with wave height, direction and period were applied on the sparse model (nested and online coupled). Main parameters for hydrodynamics, wave and sediment transport are summarized in Table 1 below:

Table 1. The main parameters of the model

Flow module		Wave module		Sediment transport module	
Parameters	Value	Parameters	Value	Parameters	Value
Δx, Δy of grid cells: (onshore; offshore)	250-350 m; 500-600 m	Computational mode	Non-stationary	Critical bed shear stress for sedimentation	0.15 N/m^2
Step time	60 sec	Coupling interval	60 minutes	Critical bed shear stress for erosion	0.25 N/m^2
Dimensional number of Sub-grid scale HLES	3	Time step	5 minutes	Erosion parameter	$1.0x10^{-5}$ $kg/m^2/s$
Horizontal Eddy Viscosity	1.0 m^2/s	Current and -type	Wave dependent	Threshold sediment layer thickness	0.05 m
Horizontal Eddy Diffusivity	10.0 m^2/s	Forces on wave energy dissipation rate 3D	On	Spin-up interval before morphological changes	720 minutes
Vertical Eddy Viscosity	$1.0x10^{-6}$ m^2/s	Generation mode for physics	3-rd generation	Specific density (non-cohesive)	2650 kg/m^3
Vertical Eddy Diffusivity	$1.0x10^{-6}$ m^2/s	Bottom friction & Coefficient	JONSWAP & 0.067 m^2s^{-3}	Dry bed density (non-cohesive)	1600 kg/m^3
Maining coefficient	0.02	Forcing	Wave energy dissipation	Median sediment diameter-Sand (D50)	200 μm
Model for 3D turbulence	k-Epsilon	Depth-included breaking (B&J model)	Alpha: 1 Gamma: 0.73		
Correction for sigma-coordinates	On	White-capping of wind	Komen et al., 1984		

Based on tidal output results from test cases, storm surge simulations began 15 days periods to the monsoon scenarios and the typhoon event of interest. Scenarios simulation is in Table 2 below:

Table 2. Simulation scenarios (online coupling of Atmosphere-Flow-Wave-Sediment model)

Simulation scenarios	Tide	Discharge	Waves	Suspended Sediment	Monsoon winds	Typhoon
(1)	Yes	Yes	Yes	Yes	Yes	-
(2)	Yes	Yes	Yes	Yes	-	Yes

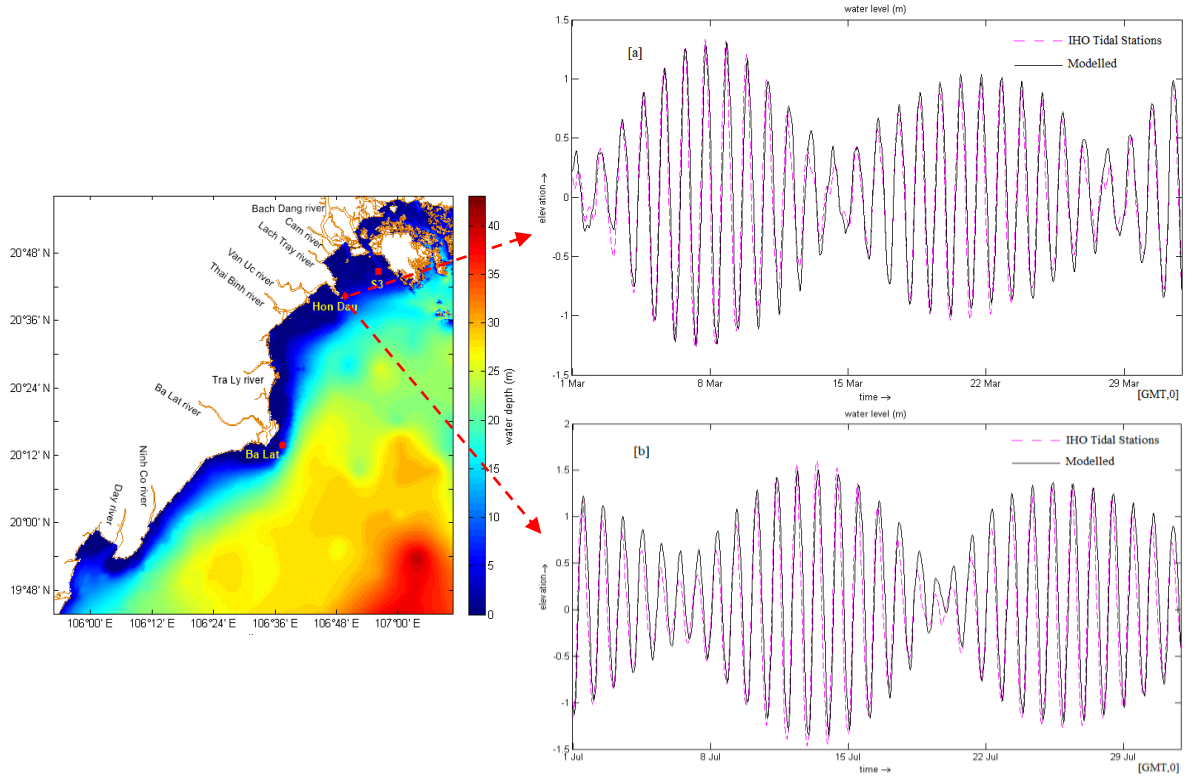

Figure 2. The comparison of modeled water level with IHO Tidal Stations at Hon Dau during the dry season [a], and wet season [b].

- Calibration and verification

In this study, we use the root mean square error (RMSE) for calibration and verification. The RMSE and is calculated for the data set as follows [19]:

$$\mathrm{RMSE} = \sqrt{\frac{\sum_{i=1}^{n}(X_{obs,i} - X_{model,i})^2}{n}} \quad (6)$$

Where $X_{obs,i}$ is observed values and $X_{model,i}$ is modeled values at time/place i.

In order to realize validation and model calibration for hydrodynamic models in GTK, we used simulated water levels to compare with observed data at Hon Dau station in the dry season of 2013 (March), and wet season of 2014 (June). Modeling results and water level data at Hon Dau station ($106^0$48'E; $20^0$40'N) have a relative agreement on both amplitude and phase (see Figure 2). Graphical comparisons indicate that the model reproduced general trends at Hon Dau station. In general, the agreement between observed and simulated data is good. Therefore, the results of hydrodynamic models could be used to set up the sediment transport model. The comparison of the results of water level shows the RMSE is the difference of 0.18 m in dry season, and difference of 0.28 m in wet season, respectively. A time series of simulated and observed current velocities at sample station Bach

Dang (Figure 3) shows that the model results match the trend and dynamics of the observed data. The comparison results of suspended sediment showed the RMSE is the difference of 0.05 m/s for dry season, and 0.09 m/s for wet season, respectively. Figure 3 presents the observed and simulated SSC at Bach Dang station (S3 station, Figure 2) for 68 hours with 4 hours interval during the wet and dry seasons, this is the period that the measured SSC data are available. The comparison results of SSC showed the RMSE is the difference of 0.01 kg/m^3 for dry season, and 0.04 kg/m^3 for wet season, respectively.

The wave height during the Super Typhoon Rammasun is also verified. The comparison of observed versus modeled wave height and wave direction at Comparisons of the predicted WAVEWATCHIII (WW3) wave height with modeled results at Northeastern of Hainan Island (110°57'18.60"E; 20°18'23.77"N) coastal area during the Super Typhoon Rammasun passage are shown in Figure 4. It can be seen from the figures that on 18th July 2014, the WW3's maximum significant wave height of 5.5 m occurred at 9h 18th July 2014, while the simulated maximum significant wave height up to 6.8 m occurred from 11:00 to 13:00. The RMSEs of the simulated wave height from the WW3 models are 0.29 m.

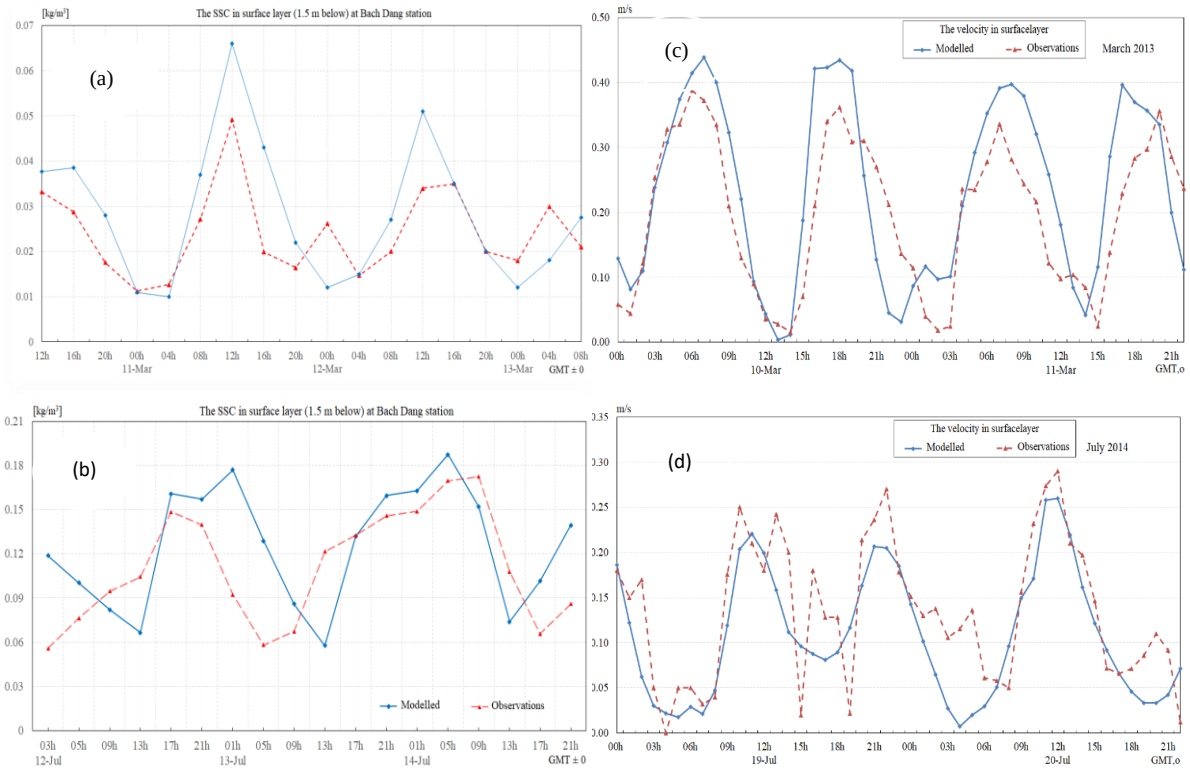

Figure 3. The comparison of observed versus modeled SSC load during dry season (a) and wet season (b); And velocity during dry season (c) and wet season (d) at the Bach Dang station.

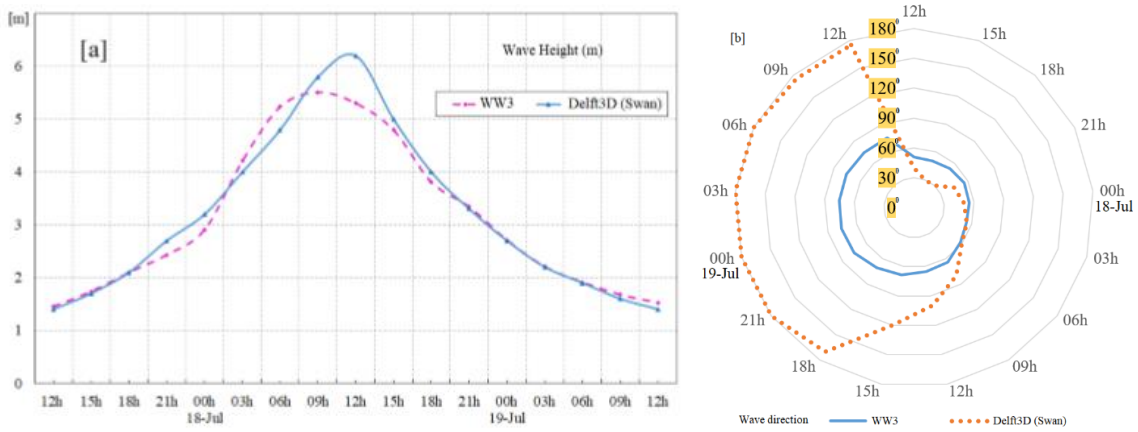

Figure 4. The comparison of the modeled versus WW3's wave height with direction during Super Typhoon Rammasun at Northeastern of Hainan Island.

Table 3. The track of the Super Typhoon Rammasun in July 2014

Time (UTC±0)	Center position		Central Pressure (hPa)	Max Wind (kt)	Time (UTC±0)	Center position		Central Pressure (hPa)	Max Wind (kt)
	Lon (E)	Lat (N)				Lon (E)	Lat (N)		
00 h-16 th	120.4	14.2	960	70	06 h-18 th	111.2	20	935	90
06 h-16 th	119	15.1	965	65	12 h-18 th	110.2	20.3	940	90
12 h-16 th	117.6	15.1	970	60	18 h-18 th	109.4	21	955	70
18 h-16 th	116.8	15.6	970	60	00 h-19 th	108.1	21.8	965	50
00 h-17 th	115.6	16.2	960	65	06 h-19 th	107	22.2	980	40
06 h-17 th	114.9	16.9	960	65	12 h-19 th	106.1	22.5	990	35
12 h-17 th	114.3	17.5	955	70	18 h-19 th	104.4	22.7	996	NaN
18 h-17 th	113.4	18.5	945	80	00 h-20 th	103.6	23	998	NaN
00 h-18 th	112.3	19.1	940	85	06 h-20 th	NaN	NaN	NaN	NaN

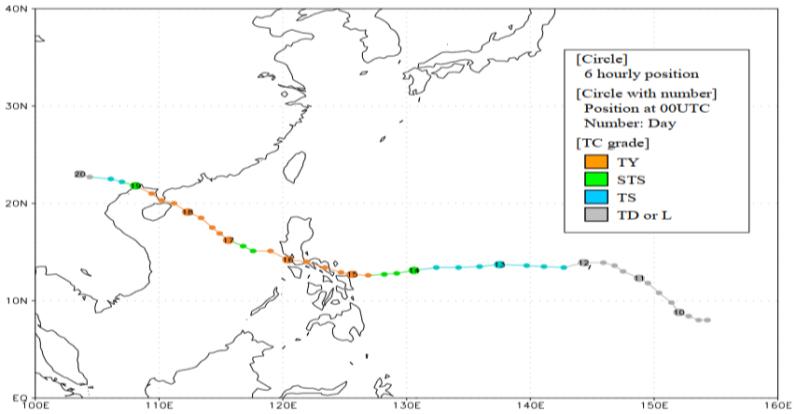

Figure 5. Track of super Rammasun Typhoon across the Phillippines and Southern China in July 2014. The points show the position of the typhoon at 6-hour intervals [8.]

2.3. Typhoon Selection

The TKG is a region with a high number of typhoon events every year, an average of almost 2.61 typhoons per year attacking and 6 typhoons per year suffering here. However, there is little has known about the relevance between the simulated typhoon and suspended sediment transport. In this study, we conducted a statistical analysis of Tropical cyclones pass through the GTK from July to September (2014), and we also examined a representative case, Super Typhoon Rammasun, which impacted strongly on the hydrodynamic and sediment transport in the coastal areas of GTK. Rammasun had destructive impacts across the Philippines, South China, and Vietnam in July 2014 (see Figure 5 and Table 3).

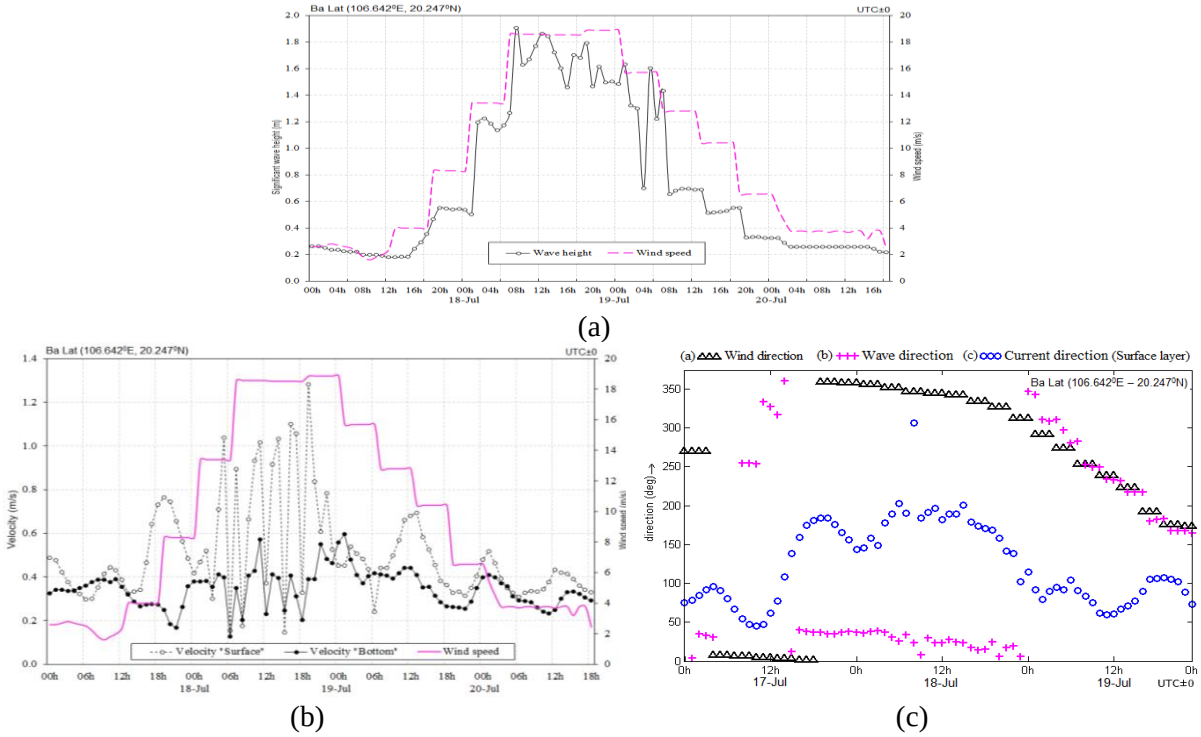

Figure 6. Response of the effective wave height (a) velocity (b) wave direction, flow direction, wind speed and wind direction (c) in the offshore waters of the Balat Estuary during typhoon.

3. Results and Discussion

i) The impacts of Rammasun Typhoon on winds

The results indicated that the average wind speed ranged from 1.5 to 4.5 m/s during the non-typhoon periods at Red River Delta coastal areas. When Rammasun Typhoon was moving across the TKG, the wind velocity increased by 6 times (Figure 6);

ii) The impacts of Rammasun Typhoon on hydrodynamics

The simulation results also show that the simultaneous incorporation of hydrodynamic-wave physical processes plays a very important role in the surges simulation. The simulation shows that, with a typhoon level of 12, the peak of wave height can increase to 6.8m compared to normal. The southeastwardly current induced by typhoon resulted in strong sea level decrease by about 0.7m in the Red River Delta coastal area during Rammasun Typhoon event (Figure 7);

To assess the impact of the typhoon on hydrodynamic conditions, we consider values of

the x- and y-components of the velocity and displacement change with time during the Rammasun Typhoon event. The characteristics of current velocity depend on atmospheric conditions, bathymetry and distance between the eye of the typhoon and the position of a region. Wind-induced surge results from a surface current generated by the friction of the water surface and wind, and it can be regarded as mass transport of water surface from offshore to onshore areas (or from onshore to offshore). Figure 8 shown a velocity component in x and y direction at a point in Ba Lat river mouth (values of the x- and y-components of the velocity and displacement change with time during the Rammasun Typhoon event). There are several mechanisms that generate extreme velocity during the Typhoon Rammasun Typhoon event from 18th to 20th July 2014 (Figure 8);

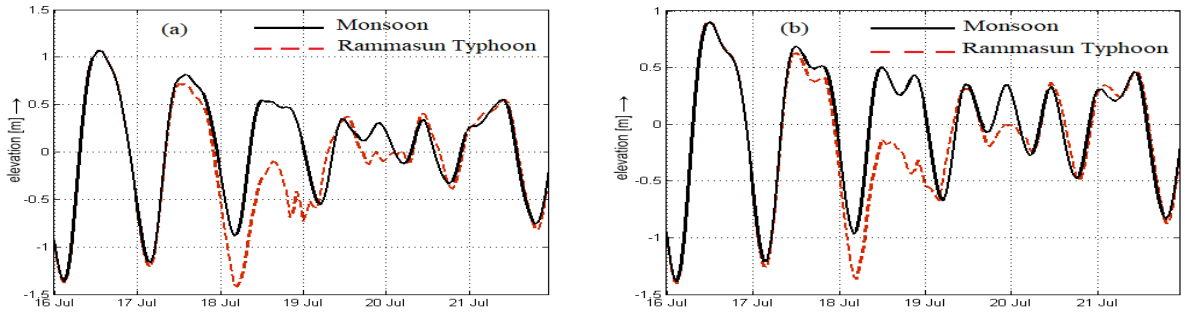

Figure 7. The modeled of the water level changes in Red River Delta coastal area (a): HonDau station and (b): BaLat estuary during Super Typhoon Rammasun event.

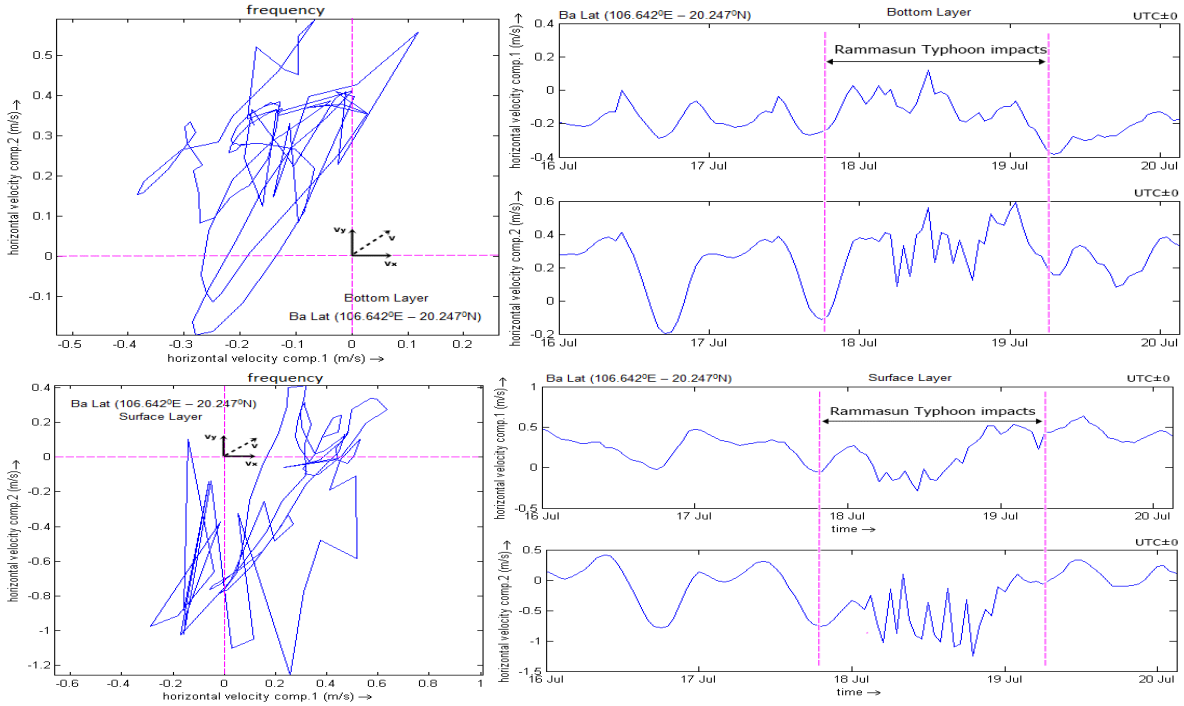

Figure 8. Modeled of velocity (x-axis to the North, y-axis to the East) in Ba Lat coastal area during Typhoon Rammasun.

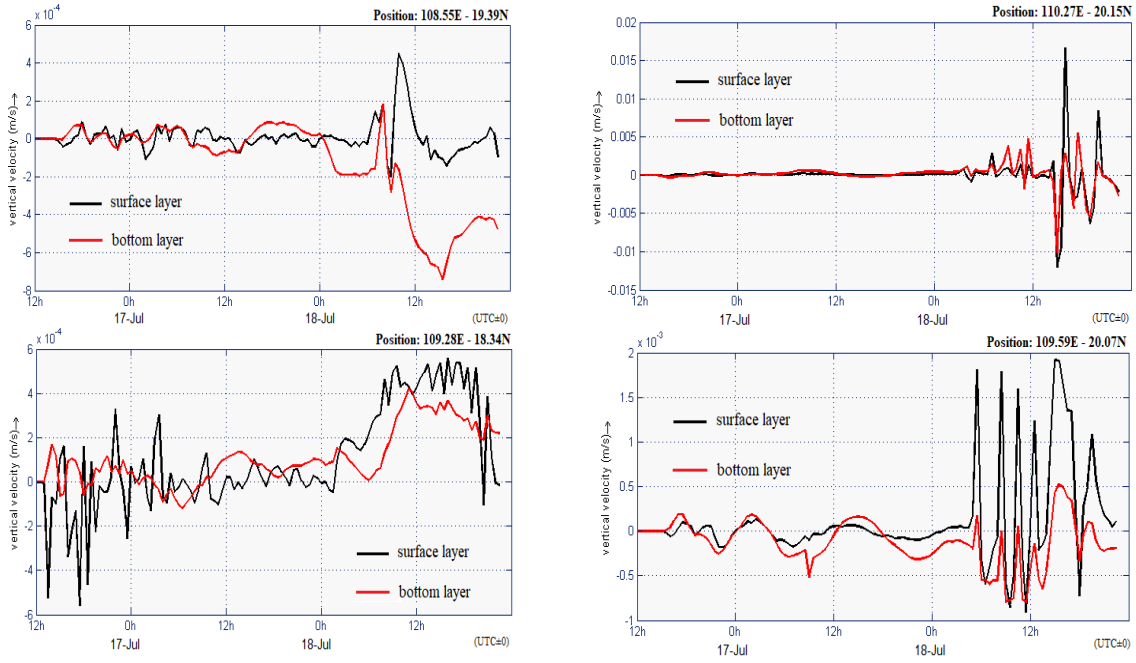

Figure 9. The modeled of vertical current velocity [m/s] during Typhoon Rammasun at some points around Hainan Island western coastal areas.

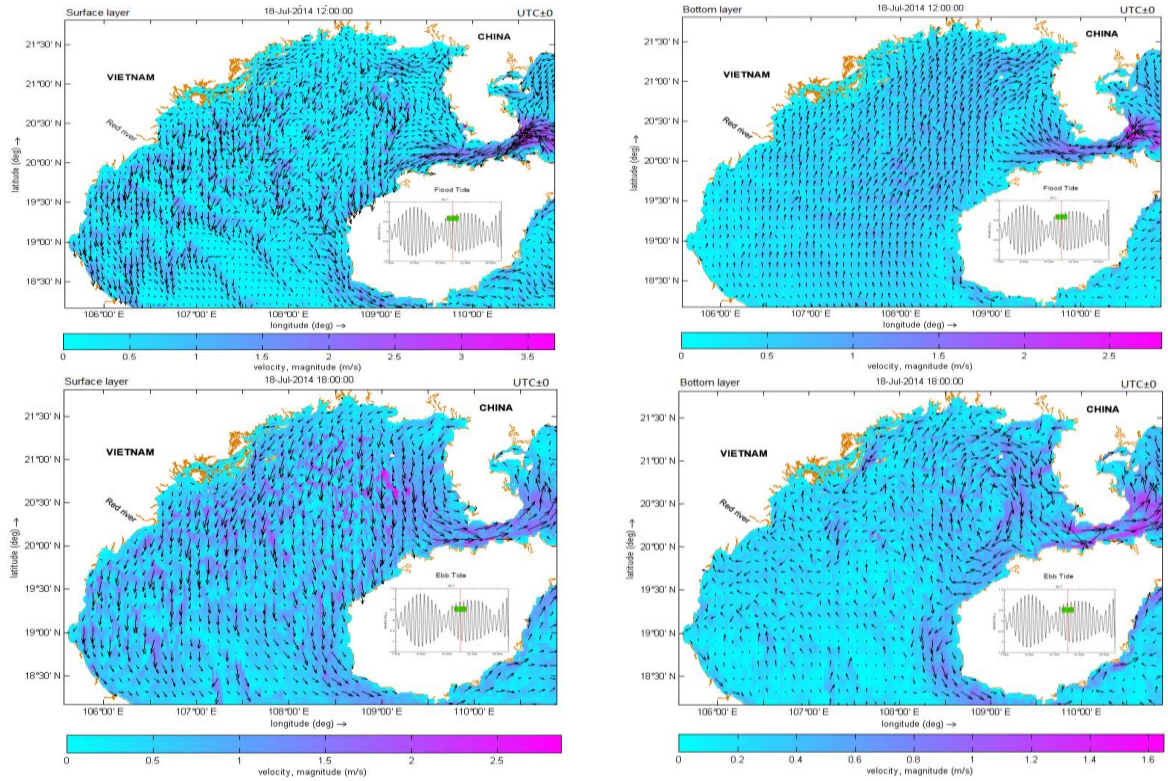

Figure 10. The modeled results of velocity field during the Typhoon Rammasun.

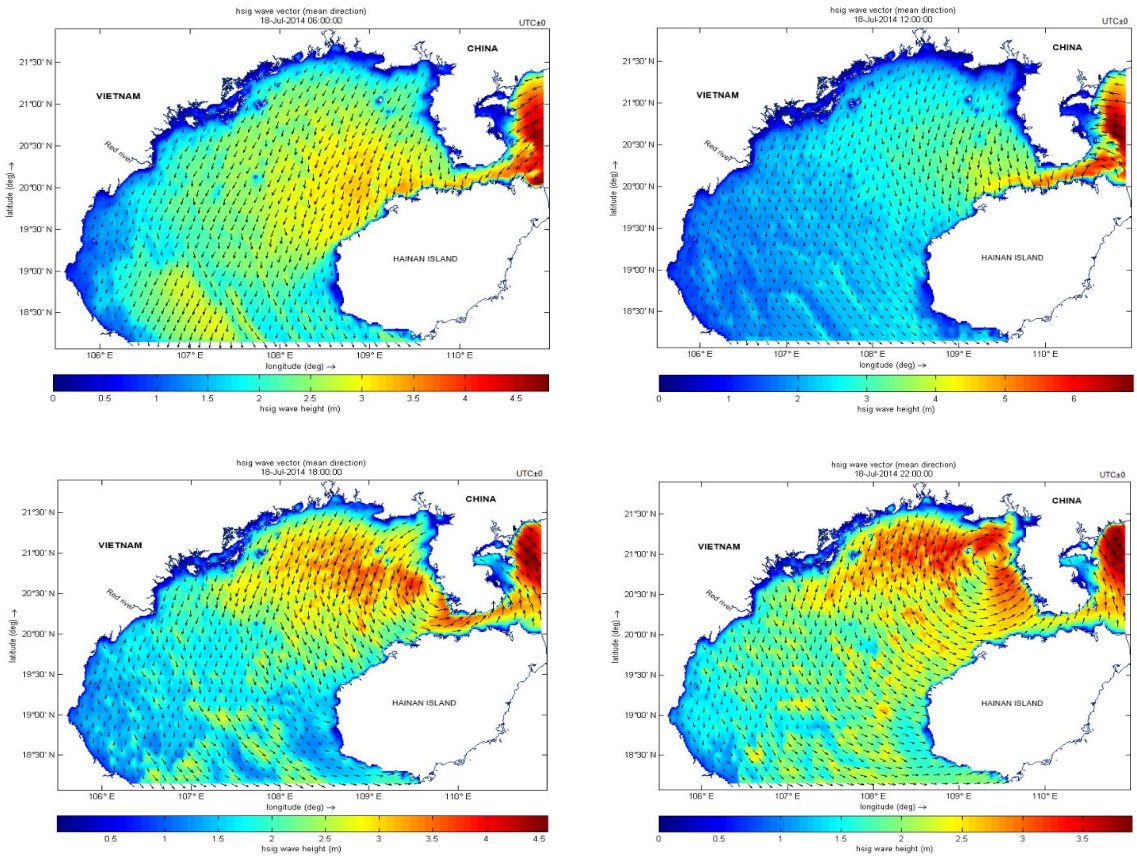

Figure 11. The modeled result of wave field during the Typhoon Rammasun.

The wind was the dominant factor driving the surface currents (wind-driven current) during the Typhoon Rammasun event in the GTK. The impact of the current velocity caused by wind is relatively similar in shallow water coastal areas, but it has more differences in the offshore area while typhoon has a little impact on velocity in the bottom layer (Figure 8, 9 and 10). In the surface layer, the current velocity was 0.25-0.3 m/s (during ebb tide stages) greater than it in normal conditions during Super Typhoon Rammasun event. This result indicates that the velocity field was periodic circulated before landfall but became unstable after the landfall.

During the time from 0h GMT 18th to 0h GMT 19th July 2014, the maximum wave height in the range of 3.6 – 6.8 m were shown during this period, and the highest wave height occurred at coastal areas of Hainan Island, mainly comprising the northeastern and northern GTK coast. But wavefield at Northwestern coastal areas of GTK (Thai Binh to Nghe An province), still reached the ranges from 0.5 to 2.0 m (see Figure 11).

iii) The impacts of Rammasun Typhoon on suspended sediment

Characteristics of sediment transport in the coastal zone of GTK are mostly controlled by hydrodynamic conditions. Sediment transported flux are prevalent moving directional alongshore. The Typhoon Rammasun activities in the study area could cause an increase of SSC around GTK coastal areas, especially there being executed typhoon in the wet season. In the wet season, influences of typhoon activities on increasing turbidity in southern areas coastal area are insignificant. During the Typhoon

Rammasun event, the values of SSC higher than it in normal conditions, and SSC value in the GTK varied dramatically in temporal and spatial distribution, with the maximum value in the wet season because of large sediment discharge around the river mouth (Figure 12 & 13);

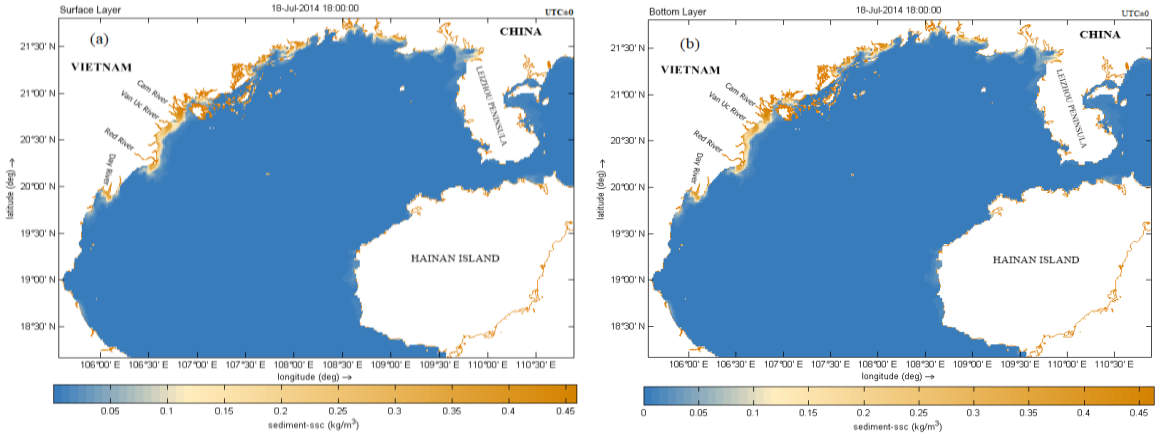

Figure 12. The modeled results of SSC transport in GTK coastal areas during Typhoon Rammasun's eye crossed the Southern China coastal area, (a)-surface layer and (b)-bottom layer.

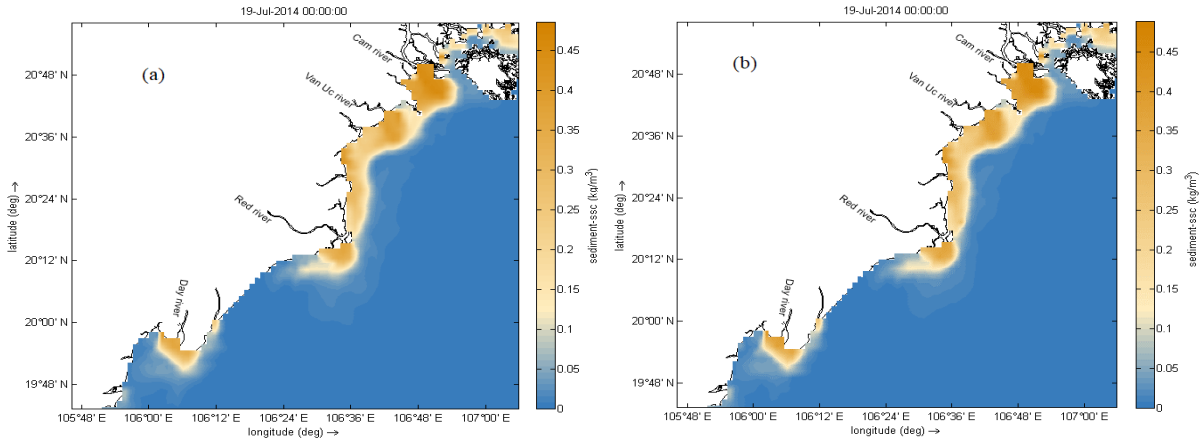

Figure 13. The modeled results of SSC transport in Red River Delta coastal area during Typhoon Rammasun's eye crossed the Southern China coastal area, (a)-surface layer and (b)-bottom layer.

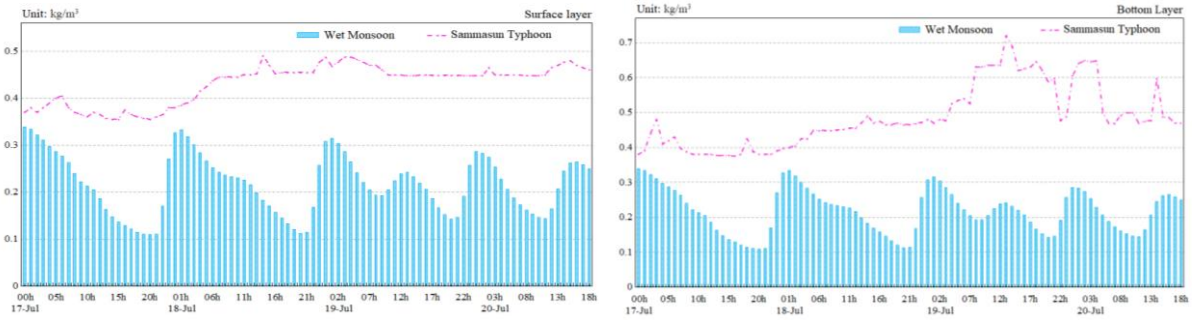

Figure 14. The modeled results of SSC with Rammasun Typhoon winds and monsoon winds conditions at Ba Lat river mouth.

This study conducted a supplementary analysis of the correlation between the wave fields in typhoons to the suspended sediment transport, by providing a statistical analysis and case study that showed the impact of TC on the SSC transport. The results showed that the calculation of simultaneous local wave properties and sediment concentration indicated a distinct correlation for situations with strong waves, but little correlation when the waves were low and most of the sediment originated from the river discharge. Otherwise, the Rammasun Typhoon occurs during the rainy season, and in the coastal zone around the Red River Delta, SSC increased with SSC vary from 0.38 to 0.49 kg/m^3 in the surface layer and SSC vary from 0.39 to 0.72 kg/m^3 in the bottom layer (Figure 14). During the Rammasun Typhoon event, the values of SSC were higher than its normal conditions and the current velocities were substantially higher during the Rammasun Typhoon event, as a result of the increased wave height.

4. Conclusion

In this study, we conducted a statistical analysis of tropical cyclones that pass through the Gulf of Tonkin from July to September (2014). The comparison of water elevation and current velocity between observation and numerical model results based on the open-source model indicated a good agreement. Thus, the model can simulate the response of the sedimentary dynamic environment to the typhoon with reasonable accuracy. The results of the simulation have provided new insight into the physical processes involved in the impact of the typhoon on suspended sediment transport. However, in terms of predictability, our study should be complemented by the investigation of a multi-model ensemble forecast for the present and other cases. In this context, the present case study opens avenues of further research to determine the frequency of such tropical–extratropical interactions and their impact on SSC transport. In order to assess the influences of typhoon activities on the morphology of the study area, it is also recommended that the simulation of other typhoon activities should be carried out in one year or in a few years. The aim of the study was to provide information on the underlying dynamics of the typhoon on suspended sediment by using numerical simulation. It was also provided with some useful understanding of the impact of the typhoon on the hydrodynamic and sediment transport in the Gulf of Tonkin.

5. Acknowledgments

This publication is resulted from the state project entitled “Scientific basics and comprehensive solution for sustainable development of Truong Sa (Spratly) District, Vietnam”, coded KC09.29/16-20; the project “Process studies on air-sea-mainland interactions and environmental variations of Bien Dong in the context of climate change within the framework of IOCIWESTPAC", code: ĐTĐL.CN-28/17”. The authors express our thanks to the project team, executing institution, Ministry of Science and Technology, Vietnam and Vietnam Academy of Science and Technology for their supports to the study.

References

[1] K. Kleinen, Historical Perspectives on Typhoons and Tropical Storms in the Natural and Socio-Economic System of Nam Dinh (Vietnam), Journal of Asian Earth Sciences. Vol. 29, 2007, pp. 523-531, https://doi.org/ 10.1016/j.jseaes. 2006.05.012.

[2] N. B. Thuy, The Risk of Typhoon and Storm Surge Along the Coast of Vietnam, Vietnam Journal of Marine Science and Technology, Vol. 19, 2019, pp. 327-336, https://doi.org/10.15625/1859-3097/19/3/13899.

[3] L. C. van Rijn, Mathematical Modeling of Morphological Processes in the Case of Suspended Sediment Transport, Thesis, Delft Tech. Univ., Delft, The Netherlands, 1987.

[4] D. B. Duy, N. D. Thanh, T. Q. Duc, P. V. Tan, Seasonal Predictions of the Number of Tropical Cyclones in the Vietnam East Sea Using Statistical

Models. VNU Jounal of Science: Earth and Environmental Sciences, Vol. 35, 2019, pp. 45-57, https://doi.org/10.25073/2588-1094/vnuees.4379.

[5] P. T. Ha, H. D. Huy, P. Q. Nam, J. Katzfey, J. McGregor, N. K. Chi, T. Q. Duc, N. M. Linh, P. V. Tan, Implementation of Tropical Cyclone Detection Scheme to CCAM Model for Seasonal Tropical Cyclone Prediction over the Vietnam East Sea, VNU Jounal of Science: Earth and Environmental Sciences,Vol. 35, 2019, pp. 49-60, https://doi.org/10.25073/2588-1094/vnuees.4384.

[6] P. Wessel, W. H. F. Smith, A Global, Self-Consistent, Hierarchical, High-Resolution Shoreline Database, J. Geophys. Res, Vol. 101, 1996, pp. 8741-8743, https://doi.org/10.1029/96JB00104.

[7] P. Weatherall, K. M. Marks, M. Jakobsson, T. Schmitt, S. Tani, J. E. Arndt, M. Rovere, D. Chayes, V. Ferrini, R. Wigley, A New Digital Bathymetric Model of the World's Oceans, Earth and Space Science, Vol. 2, 2015, pp. 331-345, https://doi.org/10.1002/2015EA000107.

[8] J. J. Becker, D. T. Sandwell, W. H. F. Smith, J. Braud, B. Binder, J. Depner, D. Fabre, J. Factor, S. Ingalls, S-H. Kim, R. Ladner, K. Marks, S. Nelson, A. Pharaoh, R. Trimmer, J. Von Rosenberg, G. Wallace, P. Weatherall, Global Bathymetry and Elevation Data at 30 Arc Seconds Resolution: SRTM30_PLUS. Marine Geodesy, An International Journal of Ocean Survey, Mapping, and Sensing, Vol. 32, 2009, pp. 355-371, hppts://doi.org/10.1080/01490410903297766.

[9] W. H. F. Smith, D. T. Sandwell, Bathymetric Prediction from Dense Satellite Altimetry and Sparse Shipboard Bathymetry, J. Geophys. Res, Vol. 99, 1994, pp. 21803-21824, hppts://doi.org/10.1029/94JB00988.

[10] W. H. F. Smith, D. T. Sandwell, Global Sea Floor Topography from Satellite Altimetry and Ship Depth Soundings, Science, Vol. 277, 1997, pp. 1956-1962, hppts://doi.org/10.1126/science.277.5334.1956.

[11] G. D. Egbert, Y. E. Svetlana, Efficient Inverse Modeling of Barotropic Ocean Tides, Journal of Atmospheric and Oceanic Technology. Vol. 19, 2002, pp. 183-204, https://doi.org/ 10.1175/1520-0426(2002)019<0183:EIMOBO> 2.0.CO;2

[12] JMA, Annual Report on the Activities of the RSMC Tokyo – Typhoon Center, Japan Meteorological Agency, Tokyo, 2014, Appendix 1, http://www.jma.go.jp/jma/jma-eng/jma center/rsmc-hp-pub-eg/AnnualReport/2014/Text/Text2014.pdf (accessed on: January 1st, 2019).

[13] WL | Delft Hydraulics, 2010. Delft3D-FLOW User Manual Version 3.04.12566. WL | Delft Hydraulics, Delft, The Netherlands, 2010.

[14] R. C. Ris, N. Booij, L. Holthuijsen, A Third-Generation Wave Model for Coastal Regions, Part I, Model Description and Validation. Vol. 104, 1999, pp. 7649-7656, https://doi.org/10.1029/98JC02622.

[15] L. Holthuijsen, N. Booij, T. Herbers, A Prediction Model for Stationary, Short-Crested Waves in Shallow Water with Ambient Currents, Coastal Engineering, Vol. 13, 1989, pp. 23-54, https://doi.org/10.1016/0378-3839(89)90031-8.

[16] J. S. Galappatti, Introduction to a Depth-Integrated Model for Suspended Transport, TUD Technical University Delft, Report, pp. 6-86, 1983.

[17] R. Galappatti, A Depth-Integrated Model for Suspended Transport, Fac. of Civ. Eng., Delft Univ. of Technol., Delft, Netherlands, 1983.

[18] R. L. Soulsby, Dynamics of Marine Sands. Thomas Telford Publishing, London, England, 1997, pp. 87-95.

[19] T. Chai, R. R. Draxler, Root Mean Square Error (RMSE) or Mean Absolute Error (MAE) – Arguments Against Avoiding RMSE in the Literature, Geoscientific Model Development, Vol. 7, 2014, pp. 1247-1250, https://doi.org/10.5194/gmd-7-1247-2014.